Check for updates

Quinoline-based fluorescent probe for the detection and monitoring of hypochlorous acid in a rheumatoid arthritis model†

Xinyi Yang,[a] Yue Wang,*[a] Zhuye Shang,[a] Zexi Zhang, [ID] [c] Haijun Chi,[b] Zhiqiang Zhang,*[b] Run Zhang [ID] [c] and Qingtao Meng [ID] *[a]

The development of effective bioanalytical methods for the visualization of hypochlorous acid (HOCl) *in situ* in rheumatoid arthritis (RA) directly contributes to better understanding the roles of HOCl in this disease. In this work, a new quinoline-based fluorescence probe (**HQ**) has been developed for the detection and visualization of a HOCl-mediated inflammatory response in a RA model. **HQ** possesses a donor−π−acceptor (D−π−A) structure that was designed by conjugating *p*-hydroxybenzaldehyde (electron donor) and 1-ethyl-4-methylquinolinium iodide (electron acceptor) through a C=C double bond. In the presence of HOCl, oxidation of phenol to benzoquinone led to the red-shift (93 nm) of the adsorption and intense quenching of the fluorescence emission. The proposed response reaction mechanism was verified by high performance liquid chromatography (HPLC) and high-resolution mass spectroscopy (HRMS) titration analysis. The remarkable color changes of the **HQ** solution from pale yellow to pink enabled the application of **HQ**-stained chromatography plates for the "naked-eye" detection of HOCl in real-world water samples. **HQ** featured high selectivity and sensitivity (6.5 nM), fast response time (<25 s) to HOCl, reliability at different pH (3.0 to 11.5) and low cytotoxicity. **HQ**'s application in biological systems was then demonstrated by the monitoring of HOCl-mediated treatment response to RA. This work thus provided a new tool for the detection and imaging of HOCl in inflammatory disorders.

Introduction

Reactive oxygen species (ROS) are important intermediates in both pathological and physiological processes of various diseases, particularly inflammatory disorders.[1–3] Among various ROS, hypochlorous acid (HOCl) and the dissociated hypochlorite ion (OCl⁻) are strong oxidants in human bodies, while this chemical has been widely used in our daily life as bleach.[4–6] In living organisms, HOCl is produced from the reaction of hydrogen peroxide (H_2O_2) and chloride ions (Cl⁻) by myeloperoxidase (MPO)-mediated catalysis.[7] The physiologically relevant levels of HOCl in living organisms are 5–25 μM. Regulated levels of HOCl in bodies could resist microbial invasion in the phagolysosome during inflammation response,[8,9] while excessive production of HOCl is implicated in a series of diseases, such as lung injuries, cardiovascular diseases, arthritis,

and even cancers.[10–13] Rheumatoid arthritis (RA) is an inflammatory joint disease leading to cartilage damage and ultimately impaired joint function.[14–16] It reported that RA affects 0.5 to 1.0% of adults in developed countries.[17]

Recent studies have found that elevated reactive oxygen species (ROS), in particular over-expressed of HOCl generation, are implicated in the pathogenesis of various inflammatory disorders.[18–21] The increasing levels of HOCl generation might be recognized as one of hallmark for inflammatory chronic arthropathies. Therefore, the development of effective bio-analytical method for the rapid and selective detection and visualization of HOCl in inflamed organisms directly contributes to better understanding the roles of this biomolecule in rheumatoid arthritis (RA) and also benefits to the assessment of the RA treatment response.[22]

Among various reported HOCl sensing methods, fluorescent imaging technology using responsive probes have attracted enormous attentions in recently years due to its unique advantages, such as high sensitivity, real-time detection, and good compatibility for bio-samples.[23–27] To date, a large number of fluorescent probes have been designed for HOCl detection *in vivo* and *in vitro* based on diverse sensing mechanisms, such as HOCl-triggered oxidation with group 16 elements,[28,29] oxime,[30,31] electron deficient C=C bonds,[32,33] *p*-methoxyphenol,[34] and *p*-alkoxyaniline.[35,36] However, the fluorescence probes that can be used for detection and visualization of HOCl-mediated

[a]*School of Chemical Engineering, University of Science and Technology Liaoning, Anshan, Liaoning, 114051, P. R. China. E-mail: qtmeng@ustl.edu.cn; Wangyue9088@163.com; Tel: +86-412-5929627*

[b]*Key Laboratory for Functional Material, Educational Department of Liaoning Province, University of Science and Technology Liaoning, Anshan, Liaoning, 114051, P. R. China. E-mail: zzq@ustl.edu.cn; Tel: +86-412-5928002*

[c]*Australian Institute for Bioengineering and Nanotechnology, The University of Queensland, Brisbane, 4072, Australia*

† Electronic supplementary information (ESI) available. See DOI: 10.1039/d1ra06224g

treatment response in RA have been scarcely reported.[37,38] Based on the specific HOCl-triggered C=C bond and C=N bond cleavage reaction, our research group have developed two HOCl-responsive fluorescence probes for the monitoring of HOCl-mediated RA in mouse model.[28,30] Following our previous studies, this work reports the development of a new fluorescence probe (**HQ**) for HOCl detection and treatment response monitoring in RA. The probe **HQ** was developed by a one-step condensation reaction between 4-hydroxybenzaldehyde and 1-ethyl-4-methyl quinolinium iodide (Scheme S1†). The probe **HQ** bearing hydroxybenzene is able to be oxidized to benzoquinone (Scheme 1A), resulting in red shift of the absorption spectra and quenching of emission. **HQ** is featured with high sensitivity and selectivity, fast response, and good biocompatibility, which allow it to be used as a tool for the monitoring of HOCl-mediated treatment response of RA in mouse model (Scheme 1B).

Results and discussion

Synthesis and characterization of HQ for HOCl detection

The probe **HQ** was synthesized by a one-step condensation reaction between 4-hydroxybenzaldehyde and 1-ethyl-4-methylquinolinium iodide. The chemical structure of **HQ** was characterized by ^{1}H NMR, ^{13}C NMR and HRMS (Fig. S1–S3†). To verify the sensing reaction mechanism, the reaction mixture of **HQ** in the presence of HOCl was determined by high performance liquid chromatography (HPLC) and HRMS. As shown in Fig. S4,† the HPLC peak at retention time of 3 min could be attributable to **HQ**. Upon the reaction with HOCl, a new peak at retention time of 2 min was emerged and **HQ**'s peak at retention time of 3 min was remarkably decreased, indicated that the reaction of **HQ** with HOCl to generate a new product. HRMS analysis of the reaction mixture showed a peak ($m/z = 276.1384$) at retention time of 2 min, which can be assigned to the oxidation product of benzoquinone derivative (Fig. S5†).[39] Therefore, the oxidation of phenol to benzoquinone was proposed as the HOCl response mechanism in this work.
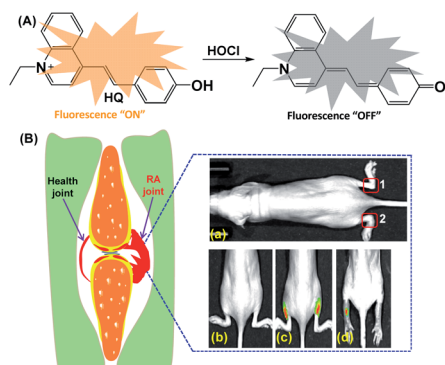
Scheme 1 (A) The proposed sensing mechanism of **HQ** to HOCl. (B) Schematic illustration of the application in the monitoring of HOCl-mediated RA model: (a) mice only. (b) Both left and right hind limbs were stimulated with λ-carrageenan and (c) followed by incubation with **HQ**. (d) The both left and right hind limbs pre-stimulated with λ-carrageenan, followed by administration with MTX (a standard therapeutic drug for RA) into the right leg and PBS into the left leg of a mouse, and finally stimulated with **HQ** in the both hind limbs.
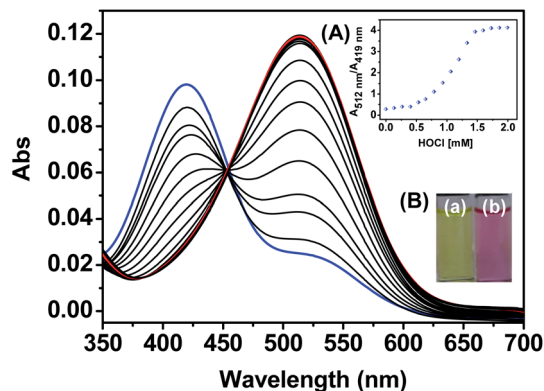
Fig. 1 Absorption spectra of **HQ** (10 μM) in the presence of increasing amounts of HOCl (0–2 mM) in PBS aqueous buffer (DMSO : H$_2$O = 1 : 9, 20 mM, pH = 7.4). Inset: (A) absorbance ratio at 512 nm and 419 nm as a function of the concentrations of HOCl. (B) Colorimetric response of **HQ** in the (a) absence and (b) presence of HOCl.

Spectroscopic responses of HQ to HOCl

As shown in Fig. 1, **HQ** exhibited an absorption band centered at 419 nm. In the presence of HOCl (0–2.0 mM), a remarkable (93 nm) red shift of the absorption spectra was observed. Specifically, the absorption at 419 nm was gradually decreased while absorption at 512 nm was gradually increased. The ratios of the absorbance ($A_{512\ nm}/A_{419\ nm}$) showed an obvious increase from 0.25 to 4.2 as the concentrations of HOCl. The change of the absorbance reached plateau upon **HQ** reacting with 1.5 mM HOCl. The bathochromic shift led to the color changes from pale yellow to pink after **HQ** reaction with HOCl. Such a dramatic color changes demonstrated that **HQ** could be used as a "naked-eye" indicator for HOCl detection. Despite remarkable changes of **HQ**'s absorption spectra to HOCl, similar changes of absorption spectra were not observed upon **HQ** reacting with 1.5 mM other species (Fig. 2A), including SO_3^{2-}, HSO_3^-, SO_4^{2-}, HSO_4^-, $ONOO^-$, $^1O_2$, HCO_3^-, $H_2PO_4^-$, $P_2O_7^{4-}$, PO_4^{2-}, S^{2-}, Br^-, Cl^-, F^-, NO_2^-, NO_3^-, OH^-, H_2O_2, Pi, CH_3COO^-, Hcy, Cys and GSH. As shown in Fig. 2B, the color changed from yellow to pink was observed upon reacting of **HQ** with HOCl only, indicating the specific UV-vis absorption response of **HQ** to HOCl.
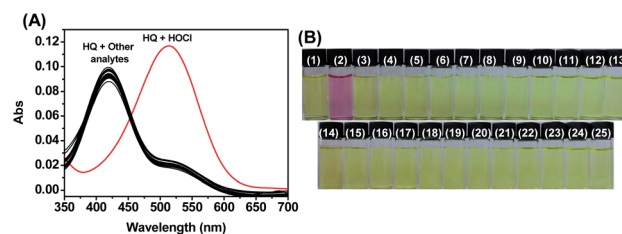
Fig. 2 (A) Absorption spectra and (B) color changes of **HQ** (10 μM) upon the addition of various analytes (1.5 mM) in PBS aqueous buffer (DMSO : H$_2$O = 1 : 9, 20 mM, pH = 7.4). (B) (1) Blank, (2) HOCl, (3) SO_3^{2-}, (4) HSO_3^-, (5) SO_4^{2-}, (6) HSO_4^-, (7) $ONOO^-$, (8) $^1O_2$, (9) HCO_3^-, (10) $H_2PO_4^-$, (11) $P_2O_7^{4-}$, (12) PO_4^{2-}, (13) S^{2-}, (14) Br^-, (15) Cl^-, (16) F^-, (17) NO_2^-, (18) NO_3^-, (19) OH^-, (20) H_2O_2, (21) Pi, (22) CH_3COO^-, (23) Hcy, (24) Cys and (25) GSH.
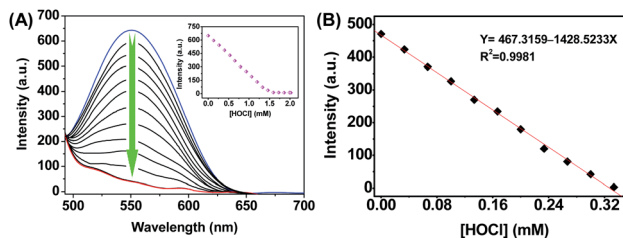
Fig. 3 (A) Fluorescence responses of **HQ** (10 μM) towards various amount of HOCl (0–2.0 mM) in PBS aqueous buffer (DMSO : H$_2$O = 1 : 9, 20 mM, pH = 7.4). Inset: fluorescence intensity of **HQ** at 550 nm as a function of HOCl. (B) The linearity between the fluorescence intensity at 550 nm and increasing HOCl concentrations (0.33 mM). Excitation was performed at 450 nm.

Next, the fluorescence response of **HQ** to HOCl was investigated. The intramolecular charge transfer (ICT)-based emission of **HQ** exhibited a strong fluorescence emission centered at 550 nm (Fig. 3A). After the reaction of **HQ** with HOCl (0 to 2.0 mM), the fluorescence was quenched and the emission intensity reached to plateau when the concentration of HOCl was 1.5 mM. In addition, the fluorescence intensity at 550 nm showed a good linearity to the concentrations of HOCl in the range of 0–0.32 mM with R^2 = 0.9981 (Fig. 3B). The limit of detection was thus calculated to be 6.5 nM based on the method defined by IUPAC.[40]

Specific fluorescence response of **HQ** to HOCl was then evaluated. As shown in Fig. 4A, distinct changes of the fluorescence intensity were not found when **HQ** reacting with 1.5 mM ROS (ONOO$^-$, ^{1}O$_2$, OH$^-$, H$_2$O$_2$), anions (SO$_3^{2-}$, HSO$_3^-$, SO$_4^{2-}$, HSO$_4^-$, HCO$_3^-$, H$_2$PO$_4^-$, P$_2$O$_7^{4-}$, PO$_4^{2-}$, S^{2-}, Br$^-$, Cl$^-$,

F$^-$, NO$_2^-$, NO$_3^-$, Pi, CH$_3$COO$^-$) and biothiols (Hcy, Cys, GSH), while remarkable changes of fluorescence signal was noticed upon reacting with HOCl. Specific fluorescence response of probe **HQ** to HOCl was also confirmed by "naked eye" fluorometric analysis, where the changes of **HQ**'s fluorescence color were observed only in the presence of HOCl (Fig. 4B). In the presence of these competitive species (1.5 mM each), the response of **HQ** to HOCl was similar to that of HOCl alone to **HQ** (Fig. 4C). The results indicate that **HQ** has excellent selectivity to HOCl over other bioactive species.

Time-/pH-dependent fluorescence response of HQ to HOCl

First, the fluorescence stability of **HQ** in PBS buffer was evaluated by measuring the emission intensity over the incubation time. As shown in Fig. S6,† the fluorescence intensities of **HQ** at 550 nm remained a constant level for 41 h, indicating the high kinetic stability of **HQ** under the test condition. Then, the time-dependent fluorescence of **HQ** to HOCl was then measured by continuously recording **HQ**'s emission intensity (λ_{em} = 550 nm) upon the addition of 0.5, 1.0 and 1.5 mM of HOCl. As shown in Fig. 5A, the fluorescence intensities of **HQ** decreased sharply upon the reaction with HOCl, and then reached a constant value until the addition of another HOCl. It is clear that the reaction of **HQ** with HOCl can be completed within 25 seconds (Fig. 5A inset), indicating the fast response of HQ to HOCl.[41–47]

Effects of pH on **HQ**'s emission and its fluorescence response to HOCl were also investigated in the presence and absence of HOCl. As shown in Fig. 5B, the fluorescence intensities of **HQ** were stable in the pH from 3 to 11.5. Upon the addition of 1.5 mM HOCl, the emission intensities of **HQ** decreased significantly and there is no obvious difference in the responses between acidic and alkaline conditions, indicating that **HQ** can be used as a fluorescence probe for HOCl detection in acidic, neutral, and alkaline conditions.

Test strips for HOCl detection in water samples

Next, the practical application of **HQ** for rapid detection of HOCl levels in real-world water samples was then evaluated.[38] **HQ**-based chromatography plates were prepared and then the plates were used for HOCl detection in real water samples. As shown in Fig. S7,† the **HQ**-based chromatography plates showed pale
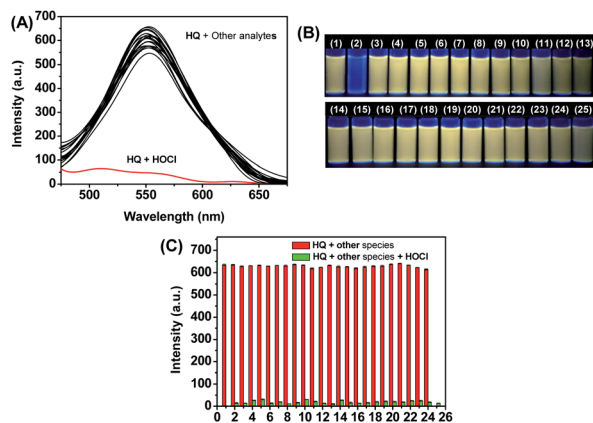

Fig. 4 (A) Fluorescence emission and (B) fluorescence color responses of **HQ** (10 μM) towards various bioactive analytes (1.5 mM) in PBS aqueous buffer (DMSO : H$_2$O = 1 : 9, 20 mM, pH = 7.4). (C) Fluorescence intensities of **HQ** (10 μM) at 550 nm in PBS aqueous buffer (DMSO : H$_2$O = 1 : 9, 20 mM, pH = 7.4) towards HOCl in the presence of diverse coexisting competitive analytes. (1) Blank, (2) SO$_3^{2-}$, (3) HSO$_3^-$, (4) SO$_4^{2-}$, (5) HSO$_4^-$, (6) ONOO$^-$, (7) ^{1}O$_2$, (8) HCO$_3^-$, (9) H$_2$PO$_4^-$, (10) P$_2$O$_7^{4-}$, (11) PO$_4^{2-}$, (12) S^{2-}, (13) Br$^-$, (14) Cl$^-$, (15) F$^-$, (16) NO$_2^-$, (17) NO$_3^-$, (18) OH$^-$, (19) H$_2$O$_2$, (20) Pi, (21) CH$_3$COO$^-$, (22) Hcy, (23) Cys, (24) GSH and (25) HOCl. Excitation was performed at 450 nm.
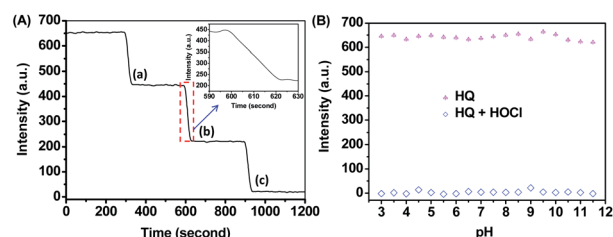

Fig. 5 (A) Time course of fluorescence response of HQ (10 μM) upon the addition of HOCl at the concentration of (a) 0.5 mM, (b) 1.0 mM and (c) 1.5 mM in PBS buffer (DMSO : H$_2$O = 1 : 9, 20 mM, pH = 7.4). (B) Influence of pH on the fluorescence emission of HQ (10 μM) in the absence and presence of HOCl. Excitation was performed at 450 nm, and emission was collected at 560 nm.
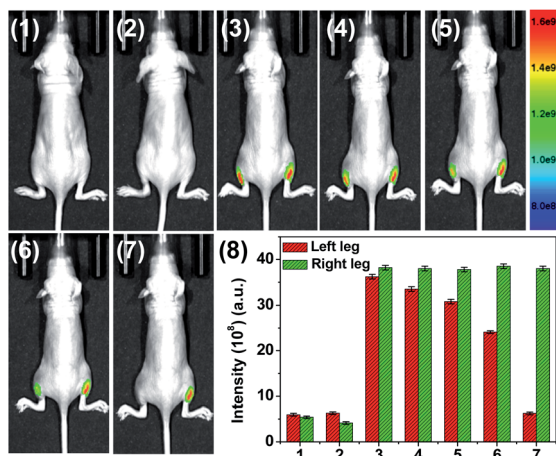
Fig. 6 Fluorescence imaging of endogenous HOCl using **HQ** in live nude mice. (1) Control group 1 (mice only), (2) left leg of the mouse was given a skin-pop injection of LPS (5 μg mL^{-1}, 80 μL) for 5 h, followed by the injection of **HQ** (20 μM, 125 μL) into the same area of the left leg. The images were then recorded at different times (3) 0.5 min, (4) 1 min, (5) 1.5 min, (6) 2 min, and (7) 2.5 min. (8) Mean fluorescence intensity analysis of HOCl in the left and right leg of the mouse at different times shown in (1–7). The right leg was injected with **HQ** (20 μM, 125 μL) only as the control group 2. Nude mice were imaged using an excitation filter (465 nm) and emission filter (570 nm).
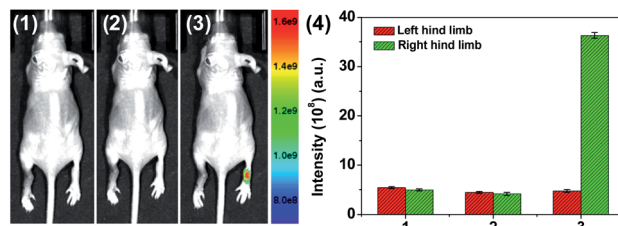

Fig. 7 Visualization of HOCl-mediated inflammatory response in RA of mice using **HQ**. (1) Control group 1 (mouse only), (2) left hind limb was stimulated with λ-carrageenan (2 μg mL^{-1}, 80 μL) in PBS for 4 h, (3) **HQ** (20 μM, 125 μL) was injected into the same area of left hind limb. (4) Mean fluorescence intensity analysis of HOCl in the left and right leg of the mouse at different times shown in (1–3). The right hind limb was injected with **HQ** (20 μM, 125 μL) only as the control group 2. Nude mice were imaged using an excitation filter (465 nm) and emission filter (570 nm).

yellow color under nature light and emitted a strong yellow fluorescence under a UV lamp (365 nm). To detect of HOCl in tap water, the chromatography plats were placed in the water samples for 5 min and then the color and fluorescence color changes were recorded. The fluorescence intensity of **HQ**-based chromatography plates decreased significantly with increasing concentration of HOCl. The colors of **HQ**-based chromatography plates changed from pale yellow to brown in two different water samples at the different concentration of HOCl (0–1.0 mM). The results demonstrated the feasibility of **HQ** for the detection of HOCl levels in water samples.

Fluorescence imaging of HOCl in live animals

Prior to the imaging of HOCl in animals, the cytotoxicity of **HQ** was evaluated by MTT assay.[48] As shown in Fig. S8,† the A549 cell viability was greater than 90% and 81% after incubation the cells with 10 μM and 20 μM **HQ** for 24 h, respectively. The result indicated that **HQ** is low cytotoxicity. The capability of **HQ** in fluorescence imaging of exogenous HOCl *in vivo* was firstly confirmed by using live nude mouse as the animal model. As shown in Fig. S9,† after subcutaneous injection of **HQ** into the left leg of a 6 to 8 week-old nude mouse, an intense fluorescence signal was detected, while fluorescence intensity was significantly decreased upon further injecting of HOCl to the same place.

Then, imaging of LPS-induced endogenous HOCl *in vivo* using **HQ** as a fluorescent imaging probe has been firstly verified in adult zebrafish.[49] As shown in Fig. S10,† silent fluorescence was observed in the **HQ**-stained group with LPS pretreatment, while strong distinct fluorescence was observed in the **HQ**-stained group. The feasibility of **HQ** for imaging endogenous HOCl was further evaluated in nude mice (Fig. 6).

LPS was injected into the left leg of the mouse. **HQ** (20 μM, 125 μL) was then injected into the same area after 5 h injection of LPS. For the control group, the same amount of **HQ** was injected into the right leg. The images were then recorded at different time courses from 0 min to 2.5 min. In the LPS-treated group, quenching of **HQ**'s fluorescence was observed for the nude mouse, while in contrast, stable and intense fluorescence was detected in the right leg without LPS treatment. The results clearly indicate that **HQ** can be used as a probe for fluorescence imaging of endogenous HOCl.

A mouse RA model was then employed to further demonstrate the application of **HQ** for imaging of HOCl-mediated inflammation response. Mouse RA model of left hind limb was obtained using previously reported procedure,[50,51] and the right hind limb was treated with PBS as the control group. **HQ** was injected into both the hind limbs at the same area, and then images were recorded immediately after injection. As shown in Fig. 7, quenching fluorescence from left ankles were obviously observed, indicating the formation of HOCl in RA. In contrast, remarkable fluorescence emission was remained for the right ankles. The results reveal that **HQ** is capable of imaging of HOCl in inflammatory tissue.

We then evaluated the capability of **HQ** for monitoring the RA treatment through assessing the HOCl-mediated fluorescence response in live mice. MTX, a standard therapeutic drug for RA patients,[52] was administered to left hind limb locally. As the control, the right hind limb was injected with same amount of PBS. Then, **HQ** was injected locally into both right and left hind limbs. As shown in Fig. 8, obvious fluorescence signal from left hind limb was appeared after MTX treatment, while weak emission was observed for the right limb where the MTX treatment were not performed. The result implies that the inhibition of HOCl generation during RA treatment.

Experimental

Synthesis of probe HQ

N-Ethyl-4-methylquinolinium iodide was synthesized following the previous report.[53] To synthesize **HQ**, *N*-ethyl-2-
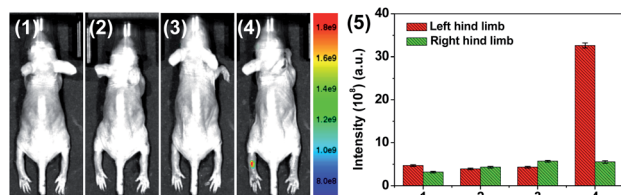
Fig. 8 Monitoring of HOCl-mediated RA treatment response using HQ. (1) Control group 1 (mouse only), (2) both left and right hind limbs were stimulated with λ-carrageenan (2 μg mL^{-1}, 80 μL) in PBS for 4 h, (3) left hind limb was administrated with MTX (20 μg in 20 μL PBS) for another 6 hour, (4) HQ (20 μM, 125 μL) was injected locally into both right and left hind limbs. (5) Mean fluorescence intensity analysis of HOCl in the left and right leg of the mouse at different times shown in (1–4). The right hind limb administrated without MTX as the control group 2. Nude mice were imaged using an excitation filter (465 nm) and emission filter (570 nm).

methylquinolinium iodide (0.299 g, 1 mmol), 4-hydroxybenzaldehyde (0.122 g, 1 mmol), and two drops of piperidine in 15 mL methanol were refluxed for 7 h. The mixture was cooled to room temperature and the solvent was removed under reduced pressure. The crude product was purified by silica column chromatography with dichloromethane–methanol (v/v, 30 : 1) as eluents. **HQ** was then obtained as a reddish brown powder in 75% yield. ^{1}H NMR (DMSO-d_6, 400 MHz): δ (ppm) 10.24 (s, 1H), 9.34 (d, $J = 6.56$ Hz, 1H), 9.06 (d, $J = 8.28$ Hz, 2H), 8.53 (d, $J = 8.88$ Hz, 1H), 8.47 (d, $J = 6.64$ Hz, 1H), 8.24 (t, $J = 7.54$ Hz, 1H), 8.13 (d, $J = 7.64$ Hz, 2H), 8.03 (t, $J = 7.68$ Hz, 1H), 7.90 (d, $J = 8.64$ Hz, 2H), 6.93 (d, $J = 8.6$ Hz, 1H), 5.01 (q, $J = 7.16$ Hz, 2H), 1.59 (t, $J = 7.16$ Hz, 3H). ^{13}C NMR (DMSO-d_6, 101 MHz), δ (ppm) 161.0, 153.7, 147.2, 144.2, 138.1, 135.5, 131.7, 129.4, 127.3, 127.0, 119.4, 116.6, 116.5, 116.1, 52.4, 15.6. ESI-MS (positive mode, m/z), calcd for $C_{23}H_{22}N_5^+$: 276.1383, [**HQ**]$^+$: found: 276.1383. Mp: 242.3–242.9 °C.

Preparation of chromatography plates for HOCl detection

The silica gel plates (25 × 75 mm) were immersed in 50 mL dichloromethane solution of **HQ** (0.5 mM) for 10 min. Then, The **HQ**-based chromatography plates were dried in air. Solutions of HOCl at different concentrations were prepared by diluting the stock solution with the water samples. The **HQ**-based chromatography plates were immersed in the HOCl aqueous solution for several seconds and then dried in air. Then, the colour changes of the **HQ**-based chromatography plates were recorded under sunlight and 365 nm UV light.

Fluorescence imaging of endogenous HOCl in adult zebrafish

All animal procedures were performed in accordance with the Guidelines for Care and Use of Laboratory Animals of Dalian Medical University and experiments were approved by the Animal Ethics Committee of University of Science and Technology Liaoning.

Adult zebrafish pre-stimulated with LPS (2 μg mL^{-1}) for 3 h and then incubated with **HQ** (20 μM) for 3 min. Zebrafish images were then recorded with an excitation filter (465 nm) and emission filter (570 nm).

Fluorescence imaging of HOCl in nude mice

The nude mice (6–8 week-old mice) were anesthetized by isoflurane in a flow of oxygen during all of the experiments. For the visualization of exogenous HOCl in live mice, **HQ** (20 μM, 125 μL) was subcutaneously injected into the lap of mouse, followed by the injection of HOCl (200 μM, 80 μL) at the same area. Images of the mouse were recorded with a 465 nm excitation filter and a 570 nm emission filter. For imaging of endogenous HOCl in living mice, LPS (5 mg mL^{-1}, 80 μL) was subcutaneously injected into the mouse left leg and the mouse was then kept for 5 h. After injection of **HQ** (20 μM, 125 μL) into this area, fluorescence imaging was conducted at different times (excitation filter 465 nm, emission filter 570 nm). The right leg of the mouse was used as the control group.

Visualization of the HOCl-mediated inflammation response in RA

The mouse RA model was obtained following the previous procedures.[28,30] **HQ** (20 μM, 125 μL) was injected into both right (without RA) and left (with RA) joints, and then fluorescence imaging was performed with a 465 nm excitation filter and a 570 nm emission filter. For monitoring of the HOCl-mediated RA treatment response, the antiarthritic drug MTX was administered locally by injection (20 μg in 20 μL PBS). At 6 h after MTX administering, **HQ** (20 μM, 125 μL) was injected locally into both right and left limbs, and then fluorescence imaging was performed after 5 min.

Conclusions

In summary, a quinoline-based fluorescence probe (**HQ**) for the detection and monitoring of HOCl-mediated inflammatory disorders in RA model was developed in this work. **HQ** showed absorption at 419 nm and yellow fluorescence centered at 550 nm. In the presence of HOCl, the oxidation of **HQ**'s phenol to benzoquinone was occurred, resulting in 93 nm red shift of the absorption spectra and the quenching of the fluorescence emission. The **HQ**-stained chromatography plates were prepared and the capability of these plates for "naked-eye" detection of HOCl in water samples was demonstrated. **HQ** was featured with high selectivity and sensitivity (6.5 nM), fast response (<25 s) and low cytotoxicity. Fluorescence imaging of exogenous and endogenous HOCl was then achieved in zebrafish and mouse models, and the capability of **HQ** for monitoring of HOCl production in mouse RA with and without MTX treatment was then successfully demonstrated. This work thus provided a new tool for the detection and visualization of HOCl in live organisms, advancing the investigations of HOCl-mediated inflammation response *in vivo*.

Author contributions

Conflicts of interest

There are no conflicts to declare.

Acknowledgements

Notes and references

1 S. J. Weiss, G. Peppin, X. Ortiz, C. Ragsdale and S. T. Test, *Science*, 1985, **227**, 747–749.

2 Y. Cui, Z. Lu, L. Bai, Z. Shi, W. Zhao and B. Zhao, *Eur. J. Cancer*, 2007, **43**, 2590–2601.

3 M. Valko, D. Leibfritz, J. Moncol, M. T. D. Cronin, M. Mazur and J. Telser, *Int. J. Biochem. Cell Biol.*, 2007, **39**, 44–84.

4 A. J. Kettle and C. C. Winterbourn, *Redox Rep.*, 1997, **3**, 3–15.

5 D. Roos and C. C. Winterbourn, *Science*, 2002, **296**, 669–671.

6 C. L. Hawkins, D. I. Pattison and M. J. Davies, *Amino Acids*, 2003, **25**, 259–274.

7 M. J. Steinbeck, L. J. Nesti, P. F. Sharkey and J. Parvizi, *J. Orthop. Res.*, 2007, **25**, 1128–1135.

8 H. Li, Z. Cao, D. R. Moore, P. L Jackson, S. Barnes, J. D. Lambeth, V. J Thannickal and G. Cheng, *Infect. Immun.*, 2012, **80**, 2528–2537.

9 J. M. McCord, *Science*, 1974, **185**, 529–531.

10 A. Daugherty, J. L. Dunn, D. L Rateri and J. W. Heinecke, *J. Clin. Invest.*, 1994, **94**, 437–444.

11 S. Hammerschmidt, N. Büchler and H. Wahn, *Chest*, 2002, **121**, 573–581.

12 Y. W. Yap, M. Whiteman and N. S. Cheung, *Cell. Signalling*, 2007, **19**, 219–228.

13 H. Zhu, J. Fan, J. Wang, H. Mu and X. Peng, *J. Am. Chem. Soc.*, 2014, **136**, 12820–12823.

14 T. B. Bennike, T. Ellingsen, H. Glerup, O. Bonderup, T. G. Carlsen, M. K. Meyer, M. Bøgsted, G. Christiansen, S. Birkelund, V. Andersen and A. Stensballe, *J. Proteome Res.*, 2017, **16**, 346–354.

15 J. S. Smolen and D. Aletaha, *Nat. Rev. Rheumatol.*, 2015, **11**, 276–289.

16 J.-T. Hou, B. Wang, Y. Zou, P. Fan, X. Chang, X. Cao, S. Wang and F. Yu, *ACS Sens.*, 2020, **5**, 1949–1958.

17 D. L. Scott, F. Wolfe and T. W. Huizinga, *Lancet*, 2010, **376**, 1094–1108.

18 X. Chen, F. Wang, J. Y. Hyun, T. Wei, J. Qiang, X. Ren, I. Shin and J. Yoon, *Chem. Soc. Rev.*, 2016, **45**, 2976–3016.

19 R. Zhang, B. Song and J. Yuan, *Trends Anal. Chem.*, 2018, **99**, 1–33.

20 S. M. Wuand and S. V. Pizzo, *Arch. Biochem. Biophys.*, 2001, **391**, 119–126.

21 B. S. Rayner, Y. Zhang, B. E. Brown, L. Reyes, V. C. Cogger and C. L. Hawkins, *Free Radicals Biol. Med*, 2018, **129**, 25–34.

22 D. D. Brand, K. A. Latham and E. F. Rosloniec, *Nat. Protoc.*, 2007, **2**, 1269–1275.

23 V. Natarajan, N. Thirumalaivasan, S.-P. Wu and V. Sivan, *Org. Biomol. Chem.*, 2019, **17**, 3538–3544.

24 J. Gong, C. Liu, S. Cai, S. He, L. Zhao and X. Zeng, *Org. Biomol. Chem.*, 2020, **18**, 7656–7662.

25 X. Cheng, H. Jia, T. Long, J. Feng, J. Qin and Z. Li, *Chem. Commun.*, 2011, **47**, 11978–11980.

26 B. Guo, H. Nie, W. Yang, Y. Tian, J. Jing and X. Zhang, *Sens. Actuators, B*, 2016, **236**, 459–465.

27 Z. Zhang, J. Fan, G. Cheng, S. Ghazali, J. Du and X. Peng, *Sens. Actuators, B*, 2017, **246**, 293–299.

28 H. Feng, Y. Wang, J. Liu, Z. Zhang, X. Yang, R. Chen, Q. Meng and R. Zhang, *J. Mater. Chem. B*, 2019, **7**, 3909–3916.

29 Q. Xu, K.-A. Lee, S. Lee, K. M. Lee, W.-J. Lee and J. Yoon, *J. Am. Chem. Soc.*, 2013, **135**, 9944–9949.

30 H. Feng, Z. Zhang, Q. Meng, H. Jia, Y. Wang and R. Zhang, *Adv. Sci.*, 2018, **5**, 1800397.

31 H. Jia, S. Xia, H. Feng, Q. Meng, C. Duan, Z. Zhang and R. Zhang, *Org. Biomol. Chem.*, 2018, **16**, 2074–2082.

32 X. Zhong, Q. Yang, Y. Chen, Y. Jiang, B. Wang and J. Shen, *J. Mater. Chem. B*, 2019, **7**, 7332–7337.

33 H. Feng, Q. Meng, Y. Wang, C. Duan, C. Wang, H. Jia, Z. Zhang and R. Zhang, *Chem.–Asian J.*, 2018, **13**, 2611–2618.

34 Z. Sun, F. Liu, Y. Chen, P. K. H. Tam and D. Yang, *Org. Lett.*, 2008, **10**, 2171–2174.

35 Y. Liao, M. Wang, K. Li, Z. Yang, J. Hou, M. Wu, Y. Liu and X. Yu, *RSC Adv.*, 2015, **5**, 18275–18278.

36 X. Zhou, Y. Jiang, X. Zhao and D. Guo, *Talanta*, 2016, **160**, 470–474.

37 W. Wu, X. Zhao, L. Xi, M. Huang, W. Zeng, J. Miao and B. Zhao, *Anal. Chim. Acta*, 2017, **950**, 178–183.

38 Q. Han, F. Zhou, Y. Wang, H. Feng, Q. Meng, Z. Zhang and R. Zhang, *Molecules*, 2019, **24**, 2455.

39 Y. Zhang, L. Ma, C. Tang, S. Pan, D. Shi, S. Wang, M. Li and Y. Guo, *Analyst*, 2016, **141**, 1859–1873.

40 L. Qiao, H. Nie, Y. Wu, F. Xin, C. Gao, J. Jing and X. Zhang, *J. Mater. Chem. B*, 2017, **5**, 525–530.

41 T. Li, L. Wang, S. Lin, X. Xu, M. Liu, S. Shen, Z. Yan and R. Mo, *Bioconjugate Chem.*, 2018, **29**, 2838–2845.

42 W. Katchamart, J. Trudeau, V. Phumethum and C. Bombardier, *Ann. Rheum. Dis.*, 2009, **68**, 1105–1112.

43 Z. Ye, R. Zhang, B. Song, Z. Dai, D. Jin, E. M. Goldys and J. Yuan, *Dalton Trans.*, 2014, **43**, 8414–8420.

44 Y.-M. Duan, S. Wang, F. Cao, Q. Zhang, S. Chen, Y.-B. Zhang, K.-P. Wang and Z.-Q. Hu, *Ind. Eng. Chem. Res.*, 2020, **59**, 992–999.

45 Y. Jiang, G. Zheng, Q. Duan, L. Yang, J. Zhang, H. Zhang, J. He, H. Sunc and D. Ho, *Chem. Commun.*, 2018, **54**, 7967–7970.

46 J. Wang, D. Cheng, L. Zhu, P. Wang, H.-W. Liu, M. Chen, L. Yuan and X.-B. Zhang, *Chem. Commun.*, 2019, **55**, 10916–10919.

47 S. Sarkar, H. Lee, H. G. Ryu, S. Singha, Y. M. Lee, Y. J. Reo, Y. W. Jun, K. H. Kim, W. J. Kim and K. H. Ahn, *ACS Sens.*, 2021, **6**, 148–155.

48 Q. Han, J. Liu, Q. Meng, Y.-L. Wang, H. Feng, Z. Zhang, Z. P. Xu and R. Zhang, *ACS Sens.*, 2019, **4**, 309–316.

49 Y. Gao, L. Zhao, J. Ma, W. Xue and H. Zhao, *Eur. J. Pharmacol.*, 2016, **780**, 8–15.

50 S. Wang, R. Chen, Q. Yu, W. Huang, P. Lai, J. Tang and L. Nie, *ACS Appl. Mater. Interfaces*, 2020, **12**, 45796–45806.

51 R. Li, Y. He, Y. Zhu, L. Jiang, S. Zhang, J. Qin, Q. Wu, W. Dai, S. Shen, Z. Pang and J. Wang, *Nano Lett.*, 2019, **19**, 124–134.

52 J. Lu, Z. Li, X. Zheng, J. Tan, Z. Ji, Z. Sun and J. You, *J. Mater. Chem. B*, 2020, **8**, 9343–9350.

53 Y. Zhang, L. Ma, C. Tang, S. Pan, D. Shi, S. Wang, M. Li and Y. Guo, *J. Mater. Chem. B*, 2018, **6**, 725–731.